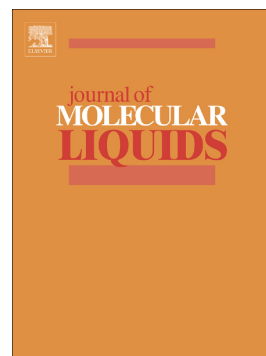


## Journal Pre-proof

The aggregation induced fluorescence effect enhanced by a reasonable length of carbon chain

Hanjun Zhang, Furong Tao, Yuezhi Cui, Zhen Xu



PII: S0167-7322(19)35532-1

DOI: <https://doi.org/10.1016/j.molliq.2020.112550>

Reference: MOLLIQ 112550

To appear in: *Journal of Molecular Liquids*

Received date: 7 October 2019

Revised date: 2 January 2020

Accepted date: 20 January 2020

Please cite this article as: H. Zhang, F. Tao, Y. Cui, et al., The aggregation induced fluorescence effect enhanced by a reasonable length of carbon chain, *Journal of Molecular Liquids*(2020), <https://doi.org/10.1016/j.molliq.2020.112550>

This is a PDF file of an article that has undergone enhancements after acceptance, such as the addition of a cover page and metadata, and formatting for readability, but it is not yet the definitive version of record. This version will undergo additional copyediting, typesetting and review before it is published in its final form, but we are providing this version to give early visibility of the article. Please note that, during the production process, errors may be discovered which could affect the content, and all legal disclaimers that apply to the journal pertain.

© 2020 Published by Elsevier.

**The Aggregation Induced Fluorescence Effect Enhanced by a  
Reasonable Length of Carbon Chain**

Hanjun Zhang, Furong Tao\*, Yuezhi Cui, Zhen Xu

School of Chemical and Pharmaceutical Engineering, Qilu University of Technology  
(Shandong Academy of Sciences), Jinan 250353, P. R. China.

Tel: +86 531 89631208; Fax: +86 531 89631760;

E-mail address: [frtao2015@126.com](mailto:frtao2015@126.com)

Journal Pre-proof

## Abstract

Six different barbituric acid derivatives using ethyl, propyl, butyl, pentyl, hexyl and heptyl groups as hydrophobic substituents were prepared. Molecular dynamics simulation was carried out to study the effect of different carbon chain lengths on the aggregation-induced emission process. Among the compounds, the CB-5 containing a hexyl substituent exhibited the strongest Aggregation induced emission (AIE) effect, not the CB-6 with longest carbon chain. The aggregates of CB-5 was used to detect the 2, 4, 6-trinitrotoluene (TNT) in aqueous media, exhibiting a maximum quenching constant of  $3.1 \times 10^5 \text{ M}^{-1}$ . The paper sensor based on CB-5 showed a superior sensitivity toward TNT both in vapor and solution. This provided a clear strategy for designing compounds that utilize the hydrophobic interaction of long-chain alkyl chains to enhance the AIE effect.

**Key words:** Aggregation induced emission; Molecular dynamics simulation; Hydrophobic interaction; Alkyl chain length

## 1. Introduction

Materials with aggregation induced emission (AIE) effect have attracted considerable research attention due to their enhanced fluorescence intensity at solid state [1, 2]. Several mechanisms have been proposed to explain the AIE phenomenon, such as restricted intramolecular rotation (RIR) [3, 4]. According to the RIR mechanism, the channel of non-radiative decay of exciton was restrained due to that the intramolecular rotation was restricted in aggregate of fluorophore molecules, thus, the emission intensity of the fluorophore was enhanced. The intermolecular actions in the aggregate, such as hydrophobic interaction, intermolecular electrostatic attraction, et al, have great impact on the RIR mechanism [5, 6].

The substituent group of alkyl has complex effect on the intermolecular action, which provides the flexibility, large steric hindrance for the molecule. In aqueous medium, the alkyl chain exhibits hydrophobic interaction between molecules. All these features contribute to the intermolecular action in the aggregate, which may have great influence on the AIE effect by affecting the RIR mechanism. Several researches about the effect of alkyl groups on the fluorescence have been reported [7-9]. Chen's team found that, as the length of the alkyl chain increases, the steric hindrance of the molecules increased and the  $\pi$ - $\pi$  stacking of intermolecular was hindered, thus the spectral shift increased and the color transition temperature decreased [10]. Wei's group discussed the effect of alkyl length on mechanofluorochromic. As the length of the alkyl chain increases, the degree of bending and deformation of the alkyl group is higher, and the crystallinity of mechanofluorochromic compounds is destroyed,

therefore the micro-morphology of aggregate remains almost unchanged before and after the grinding, which weakens the property of mechanofluorochromic [11]. These reports mainly discussed about the influence of the flexibility and steric hindrance of alkyl groups on the optical properties of the AIE aggregate. However, the effect of hydrophobic interaction of the alkyl group on the AIE activity of aggregate in aqueous medium have seldom been reported.

In this work, a series of barbituric acid derivatives by conjugating carbazole and barbituric acid have been synthesized, in which, various alkyl substituents were attached on the N-atom of carbazole (Scheme 1). In these compounds, two kinds of intermolecular actions may exist: i) the intermolecular electrostatic attraction between the carbazole and the barbituric acid moieties is due to that the carbazole moiety is electron-rich aromatic ring and the barbituric acid moiety is electron-deficient; ii) the alkyl chain structure of the compounds induce the intermolecular hydrophobic action. To study the relationship between AIE effect and molecule structure will provide useful strategy for designing molecule with excellent AIE effect. Additionally, one of the compounds synthesized in this work (CB-5) showed excellent sensing performance to 2,4,6-trinitrotoluene (TNT), which may be a promising candidate for TNT sensor.

## **2. Experimental section**

### **2.1. Materials**

1,3-dimethyl-barbituric acid, Carbazole, 1-Bromoethane, 1-Bromopropane, 1-Bromobutane, 1-Bromopentane, 1-Bromohexane and 1-Bromononane (A.R., 99%) were purchased from Energy, and which were used without further purification. DMF

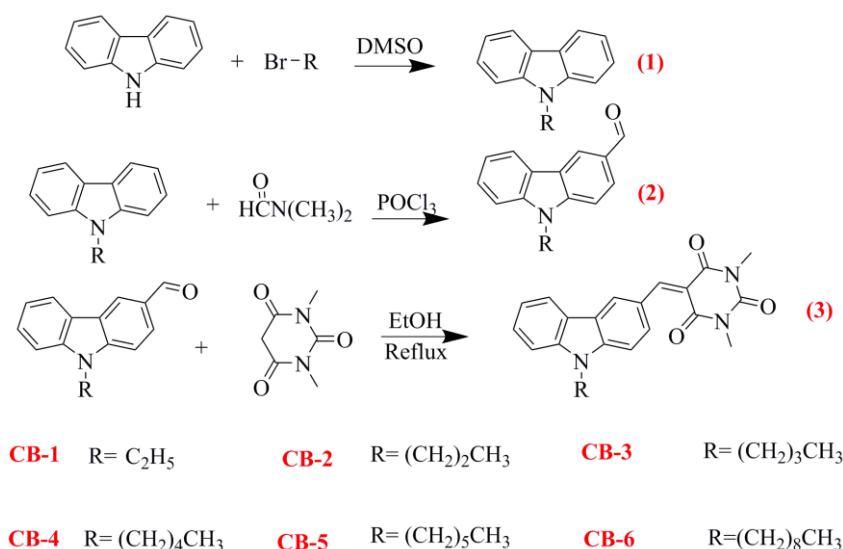
was dried sequentially by molecular sieves (4 Å), CaH<sub>2</sub>, sodium sand and distilled prior to use.

## 2.2. Measurements

Emission spectra, UV-vis spectra, <sup>1</sup>H NMR (600 MHz) spectra were recorded by F-4600 fluorescence spectrophotometer, UV-2500 spectrometer and AVANCE II 400 spectrometer, respectively. FT-IR spectra were recorded by a Nicolet 380 spectrometer.

## 2.3. Synthesis

The six compounds in this paper 1,3-dimethyl-5-((9-ethyl-9H-carbazol-3-yl)methylene)pyrimidine-2,4,6-trione (CB-1), 1,3-dimethyl-5-((9-propyl-9H-carbazol-3-yl)methylene)pyrimidine-2,4,6-trione (CB-2), 1,3-dimethyl-5-((9-butyl-9H-carbazol-3-yl)methylene)pyrimidine-2,4,6-trione (CB-3), 1,3-dimethyl-5-((9-amyl-9H-carbazol-3-yl)methylene)pyrimidine-2,4,6-trione (CB-4), 1,3-dimethyl-5-((9-hexyl-9H-carbazol-3-yl)methylene)pyrimidine-2,4,6-trione (CB-5), 1,3-dimethyl-5-((9-nonyl-9H-carbazol-3-yl)methylene)pyrimidine-2,4,6-trione (CB-6) were successfully synthesized. The structure of all compounds was proved by <sup>1</sup>H NMR spectra and FT-IR spectra. The synthesis of compounds (1) and (2) in Scheme 1 were according to ref. [12].



**Scheme 1** Synthetic routes of CB-1, -2, -3, -4, -5 and -6.

**Synthesis Procedure:** A mixture of compound (2) (3 mmol) and 1,3-dimethylbarbituric acid (3 mmol) in ethanol (10 ml) was refluxed for 4 hours, the filtrate was concentrated under reduced pressure and further purified by column chromatography (Ethyl acetate: petroleum ether =1:5; Yield: 90%).

**CB-1:** <sup>1</sup>H NMR (400 MHz, Chloroform-*d*) δ 9.28 (s, 1H), 8.81 (s, 1H), 8.55 (d, *J* = 8.8 Hz, 1H), 8.22 (d, *J* = 7.8 Hz, 1H), 7.59-7.51 (m, 1H), 7.47 (dd, *J* = 8.5, 5.1 Hz, 2H), 7.36 (t, *J* = 7.5 Hz, 1H), 4.43 (q, *J* = 7.3 Hz, 2H), 3.47 (s, 6H), 1.50 (t, *J* = 7.2 Hz, 3H) (Fig. S1). FT-IR (KBr): 3065 cm<sup>-1</sup> (=C-H), 1667 cm<sup>-1</sup> (C=O) (Fig. S2).

**CB-2:** <sup>1</sup>H NMR (400 MHz, Chloroform-*d*) δ 9.29 (s, 1H), 8.81 (s, 1H), 8.54 (d, *J* = 8.9 Hz, 1H), 8.22 (d, *J* = 7.7 Hz, 1H), 7.54 (t, *J* = 7.7 Hz, 1H), 7.47 (dd, *J* = 8.6, 3.3 Hz, 2H), 7.35 (t, *J* = 7.5 Hz, 1H), 4.33 (t, *J* = 7.1 Hz, 2H), 3.47 (s, 6H), 1.96 (p, *J* = 7.5 Hz, 2H), 1.01 (t, *J* = 7.4 Hz, 3H) (Fig.S3). FT-IR (KBr): 3005 cm<sup>-1</sup> (=C-H), 1665 cm<sup>-1</sup> (C=O) (Fig. S4).

**CB-3:** <sup>1</sup>H NMR (400 MHz, Chloroform-*d*) δ 9.28 (s, 1H), 8.81 (s, 1H), 8.55 (d, *J* = 8.8 Hz, 1H), 8.21 (d, *J* = 7.8 Hz, 1H), 7.61-7.33 (m, 4H), 4.36 (s, 2H), 3.47 (s, 6H), 1.90 (p, *J* = 7.4 Hz, 2H), 1.43 (q, *J* = 7.4 Hz, 2H), 0.98 (t, *J* = 7.3 Hz, 3H) (Fig. S5). FT-IR

(KBr): 2899  $\text{cm}^{-1}$  (=C-H), 1671  $\text{cm}^{-1}$  (C=O) (Fig. S6).

**CB-4:**  $^1\text{H}$  NMR (400 MHz, Chloroform-*d*)  $\delta$  9.28 (s, 1H), 8.81 (s, 1H), 8.55 (d,  $J = 8.8$  Hz, 1H), 8.21 (d,  $J = 7.8$  Hz, 1H), 7.62-7.33 (m, 4H), 4.35 (t,  $J = 7.2$  Hz, 2H), 3.47 (s, 6H), 1.91 (d,  $J = 7.5$  Hz, 2H), 1.44 - 1.31 (m, 4H), 0.91 (d,  $J = 6.8$  Hz, 3H) (Fig. S7).

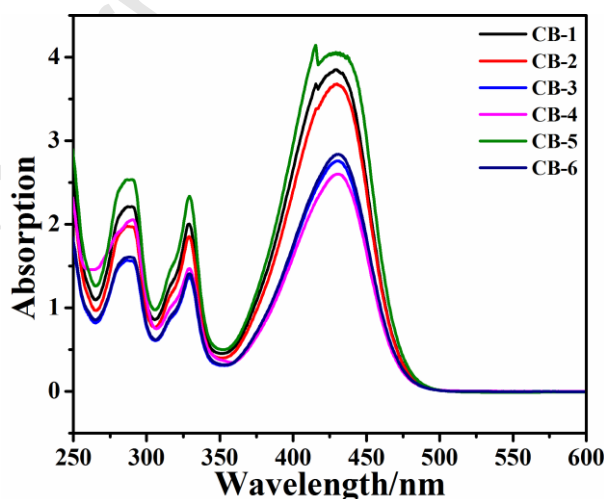
FT-IR (KBr): 2900  $\text{cm}^{-1}$  (=C-H), 1677  $\text{cm}^{-1}$  (C=O) (Fig. S8).

**CB-5:**  $^1\text{H}$  NMR (400 MHz, Chloroform-*d*)  $\delta$  9.28 (s, 1H), 8.81 (s, 1H), 8.55 (d,  $J = 8.9$  Hz, 1H), 8.21 (d,  $J = 7.8$  Hz, 1H), 7.62 - 7.33 (m, 4H), 4.35 (t,  $J = 7.3$  Hz, 2H), 3.47 (s, 6H), 2.06 - 1.77 (m, 2H), 1.48 - 1.24 (m, 6H), 0.88 (t,  $J = 6.9$  Hz, 3H) (Fig. S9). FT-IR (KBr): 2900  $\text{cm}^{-1}$  (=C-H), 1665  $\text{cm}^{-1}$  (C=O) (Fig. S10).

**CB-6:**  $^1\text{H}$  NMR (400 MHz, Chloroform-*d*)  $\delta$  9.28 (s, 1H), 8.81 (s, 1H), 8.55 (d,  $J = 8.9$  Hz, 1H), 8.21 (d,  $J = 7.8$  Hz, 1H), 7.47 (d,  $J = 3.8$  Hz, 4H), 4.34 (t,  $J = 7.2$  Hz, 2H), 3.47 (s, 6H), 2.05 - 1.81 (m, 2H), 1.31 (d,  $J = 45.6$  Hz, 12H), 0.87 (t,  $J = 6.7$  Hz, 3H) (Fig. S11). FT-IR (KBr): 2988  $\text{cm}^{-1}$  (=C-H), 1666  $\text{cm}^{-1}$  (C=O) (Fig. S12).

### 3. Results and discussion

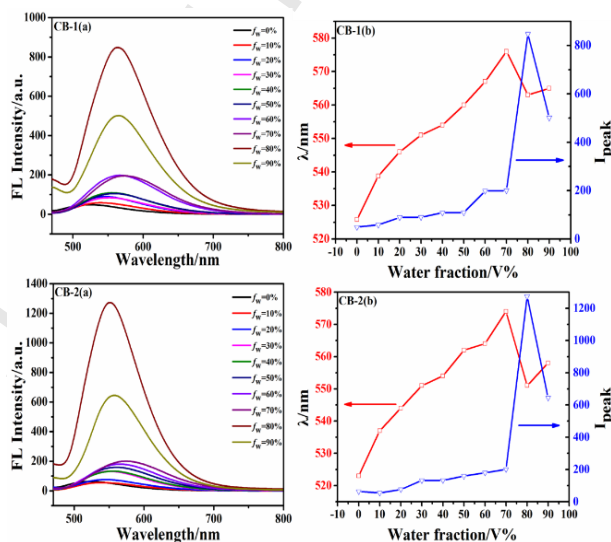
#### 3.1 Optical properties



**Fig. 1** UV-visible absorption spectra of CB-1, -2, -3, -4, -5 and -6 in THF solution ( $10^{-4}\text{M}$ )

The absorption spectra of the six barbituric acid derivatives are shown in Fig. 1. The absorption peaks in the wavelength range from 400 to 500 nm was attributed to the intramolecular charge transfer (ICT) from the carbazole unit to the barbituric acid unit, and those in the range between 250 to 350 nm are belong to  $\pi$ - $\pi^*$  electronic transition [13]. Additionally, the absorption peaks of the six compounds are basically similar to each other, indicating that the length of the hydrocarbon chains on N-atom does not change the conjugated system of the barbituric acid derivatives in pure THF. It is also noted that the absorption intensity is affected by the length of the alkyl chain, the trend was that as the alkyl chain grows, the absorption intensity decreases. The reason may be that as the length of alkyl chain grows, the host molecule is entangled by alkyl chain, which reduces the absorbance. However, it is also found that CB-5 exhibits the highest absorption intensity, which may be due to the special structure of CB-5 itself.

### 3.2 AIE activity



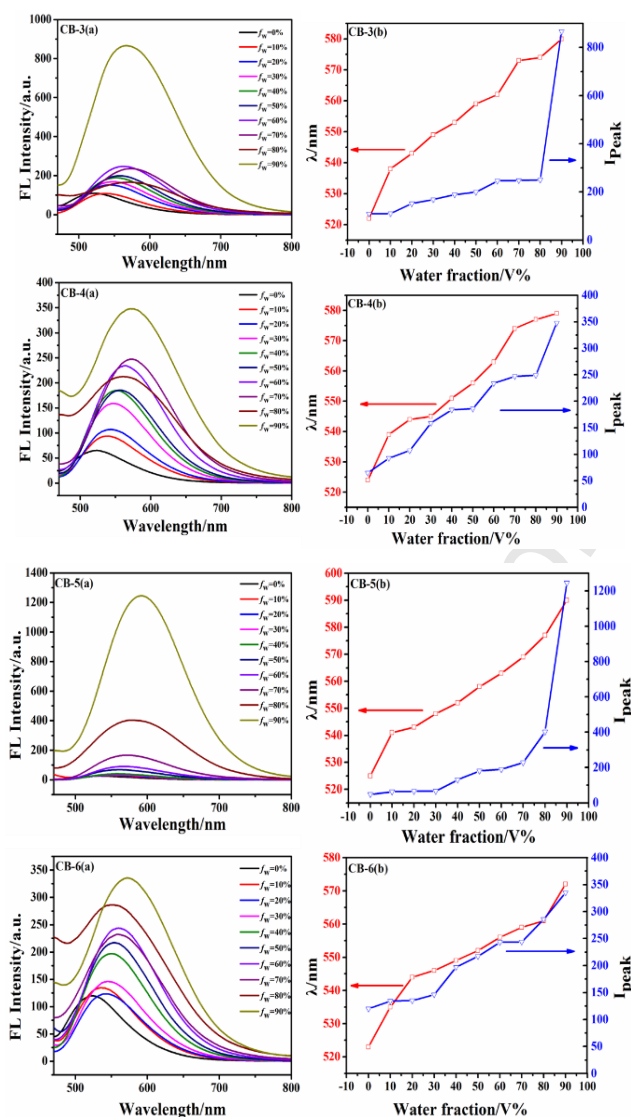


**Fig. 2** (a): Fluorescence spectra of CB-1, -2, -3, -4, -5, and -6 in different water content ( $f_w$ ) of THF/H<sub>2</sub>O mixture ( $10^{-4}$  M); (b): emission peak (red) and emission intensity (blue) relative to the water fraction in the mixture.

All the compounds exhibited weak fluorescence intensity in pure THF. However, when in the mixed THF/H<sub>2</sub>O solvents, they all emitted the enhanced fluorescence, indicating all the compounds were AIE active. The fluorescence spectra of these compounds were measured in THF/H<sub>2</sub>O by changing the water fraction ( $f_w$ ), as shown in Fig. 2 (a). Moreover, the curves of fluorescence peak wavelength ( $\lambda_{em}$ ) verse  $f_w$ , as well as those of fluorescence peak intensity ( $I_{em}$ ) verse  $f_w$ , were analyzed in Fig. 2 (b).

All the six compounds are well dissolved in THF. In pure THF, the free rotation of certain bonds of the molecule dissipates the excited state energy, making the fluorescence weak. As water is added to the THF, the compounds gradually aggregate in the mixed solvent, due to that water is poor solvent for these compounds. Meanwhile, the strong interaction between the molecules in the aggregates restricted the free rotation of the chemical bonds in the molecules, and suppressed the non-radiative transition channel, thus the fluorescence is enhanced. As shown in Fig. 2, the fluorescence intensity of CB-3, -4, -5 and -6 increases monotonously with the  $f_w$  increasing. Moreover, the  $\lambda_{em}$  of the four compounds also exhibits monotonous increasing trend as the water fraction of THF/H<sub>2</sub>O mixture increased. These results indicate that interaction between molecules in the aggregates gradually enhanced, resulting in AIE enhancement and red shift of the fluorescence spectra.

However, the changing trend of fluorescence intensity of CB-1 and -2 is complicated. When the  $f_w$  increases from 0% to 70%, the fluorescence intensity increases with the  $f_w$  increasing, accompanied by the red shift of  $\lambda_{em}$ . Because interaction between molecules in the aggregates gradually enhanced, resulting in AIE enhancement and red shift of the fluorescence spectra. When  $f_w$  increases from 70% to 80%, the intensity of the fluorescence still rises, however, accompanied by a blue shift of  $\lambda_{em}$ . This result is due to the molecules aggregate in larger size with the  $f_w$  of 70% to 80%, and the intramolecular micropolarity is lowered, leading to blue shift of  $\lambda_{em}$  [14, 15]. when  $f_w > 80\%$ , the amorphous particles form in solution leading to red shifted of  $\lambda_{em}$ .

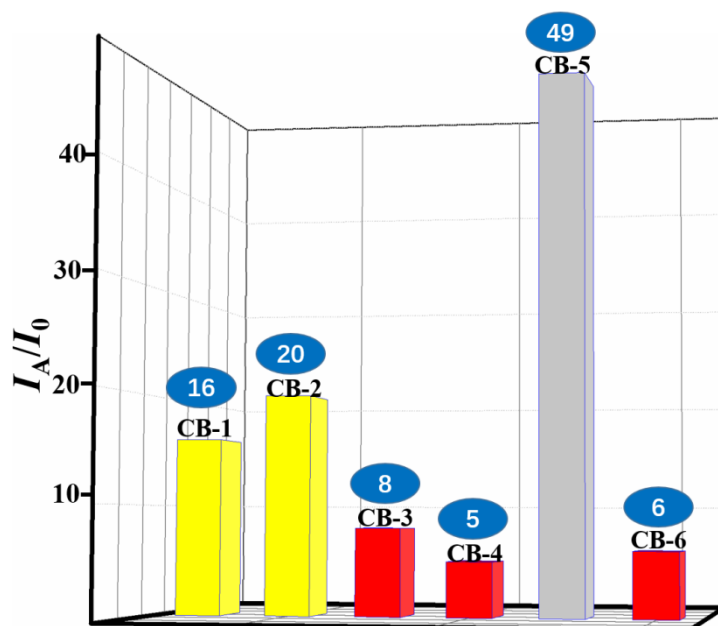


**Fig. 3** The AIE index of CB-1, -2, -3, -4, -5 and -6.

The AIE index ( $I_A/I_0$ ) is used to quantify the AIE activity, in which,  $I_A$  is the maximum fluorescence intensity of the molecule aggregation in THF/H<sub>2</sub>O ( $0 < f_w < 100\%$ ), while  $I_0$  is the fluorescence intensity when  $f_w = 0\%$ . As shown in Fig. 3, the AIE index of CB-1, -2, -3, -4, -5 and -6 is 16, 20, 8, 5, 49 and 6, respectively. The AIE index of these compounds decreases in the following sequence: CB-5 > CB-2 > CB-1 > CB-3 > CB-6 ~ CB-4. Obviously, the compound CB-5 shows the strongest AIE activity.

The Fluorescence quantum yields of aggregate state are determined relative to coumarin 307 in ethanol solution as a quantum yield standard ( $\Phi_F$  (Fluorescence quantum yield) = 56%). The coumarin 307 is selected as a standard to study the  $\Phi_F$  due to its maximum absorption and emission wavelength (395 nm and 500 nm, respectively), which are close to the synthesized AIE compounds in this work. As shown in Table 1, the fluorescence quantum yield of these compounds in the aggregated state decreases in the following order: CB-5 > CB-2 > CB-1 > CB-3 > CB-6

~CB-4. Obviously, the CB-5 with the strongest AIE activity exhibits the highest fluorescence quantum yield in the aggregated state.

**Table 1** The fluorescence quantum yield of all compounds in the aggregated state.

	CB-1	CB-2	CB-3	CB-4	CB-5	CB-6
Aggregates $\Phi_F$ (%)	7.9	8.5	3.2	2.1	11.2	1.9

As shown in Fig. S13, at aggregate state, the average diameters of the nanoaggregates for CB-1~6 are 106.4, 103.2, 122.6, 142.5, 91.6 and 156.4 nm, respectively. The size of nanoaggregates in the aggregated state increases in the following order: CB-5 < CB-2 < CB-1 < CB-3 < CB-6 ~ CB-4. (Table 2). The results indicate that the size of CB-5 in the aggregated state is the smallest and the most tightly combined, which is confirmed by MD. The Hydrophobic and electrostatic interactions work together to restrict the rotation of certain bonds in CB-5, limit the non-radiative transition channels, and result in the strongest AIE activity and the highest fluorescence quantum yield. These data indicate that the enhanced emission of compounds is related to the formation of nanoaggregates.

**Table 2** Average diameter of nanoaggregates in the aggregated state of compounds.

	CB-1	CB-2	CB-3	CB-4	CB-5	CB-6
average diameters (nm)	106.4	103.2	122.6	152.5	91.6	156.4

### 3.3 Aggregation structures from molecular dynamics simulations

In order to better understand the relationship between the AIE index and the molecule structure, the molecular dynamics (MD) simulations were performed for the

six compounds through the Materials Studio software (Accelrys Inc). For each compound (CB-1, CB-2, CB-3, CB-4, CB-5, and CB-6), four molecules of each compound were randomly dissolved in 200 water molecules, respectively, to form 6 different initial systems with the same cubic simulation lattice ( $x = 20.83 \text{ \AA}$ ,  $y = 20.83 \text{ \AA}$ , and  $z = 20.83 \text{ \AA}$ ). The simple point charge (SPC) model [16, 17], which can accurately describe the water solution environment [18], is adopted for all water molecules.

The MD simulation was performed after charges and potentials were assigned to each atom. The long-range electrostatic interactions have been accounted for using the Ewald method. The total energy is written as a combination of valence terms including diagonal and off-diagonal cross-coupling terms and nonbond interaction terms, the coulombic and Lennard-Jones functions for electrostatic and van der Waals interactions (eq. 1).

$$E = E_{\text{bonds}} + E_{\text{angles}} + E_{\text{dihedrals}} + E_{\text{cross}} + E_{\text{VDW}} + E_{\text{elec}} \quad (1)$$

Where  $E_{\text{VDW}}$  and  $E_{\text{elec}}$  are given by the eq. 2:

$$E_{\text{non-bond}} = E_{\text{VDW}} + E_{\text{elec}} = \sum \varepsilon_{ij} \left[ 2 \left( \frac{\sigma_{ij}}{r_{ij}} \right)^9 - 3 \left( \frac{\sigma_{ij}}{r_{ij}} \right)^6 \right] + \sum \frac{q_i q_j}{r_{ij}} \quad (2)$$

The parameters for each like-site interaction are given by the COMPASS force field [19, 20]. The energies of the initial configurations for each system were minimized with the Smart Minimizer method. After the minimization, this simulations were equilibrated at constant temperature (298.15 K) and volume (NVT) for 10 ns. Atomic coordinates were saved for every 200ps.

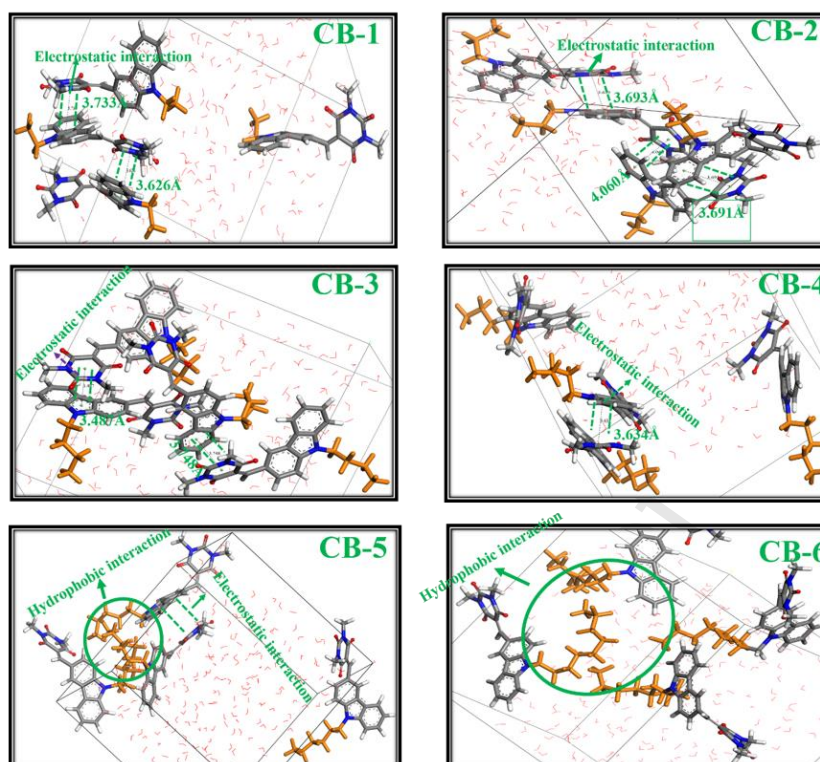


**Fig. 4** Molecular dynamics simulations were performed for CB-1, -2, -3, -4, -5 and -6 different systems through the Materials Studio software (Accelrys Inc).

The aggregation structures of the six compounds are shown in Fig. 4. For the aggregates of the compounds CB-1 and CB-2, the alkyl chains on the N-atom are localized in adverse ends of two neighbouring molecules, indicating there is no hydrophobic interaction between molecules, due to that alkyl chain on the N-atom is relatively short ( $C_2H_5$  and  $n-C_3H_7$  for CB-1 and CB-2, respectively). However, because the carbazole ring is an electron-rich aromatic ring, and the barbituric acid moiety is an electron-deficient six-membered ring, thus the two adjacent molecules are gathered together by the strong intermolecular electrostatic attraction which limits the rotation of the intramolecular bonds and leads to the strong AIE effect. As observed in Fig. 4, the molecular aggregation of CB-2 is more compact than that of CB-1, indicating the

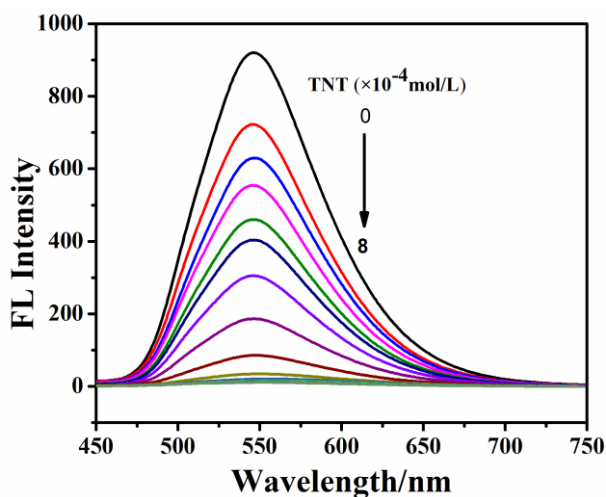
intermolecular electrostatic attraction in the compound CB-2 is stronger. Therefore, CB-2 exhibits larger AIE index than CB-1.

Similarly, the alkyl chain on the N-atom in CB-3 and CB-4 are also localized in different directions, implying no strong hydrophobic interaction between molecules. The intermolecular electrostatic attraction between the carbazole ring and the barbituric acid ring also exists in the aggregates, resulting in the AIE effect of both CB-3 and CB-4. However, because the space volumes of the alkyl chain on the N-atom ( $n\text{-C}_4\text{H}_9$  and  $n\text{-C}_5\text{H}_{11}$  for CB-3 and CB-4, respectively) are larger than those of CB-1 and CB-2, which hinders the formation of closer packing between molecules CB-3 and CB-4, thus CB-3 and CB-4 show relatively small AIE index than that of both CB-1 and CB-2.

In CB-5 aggregates, the alkyl chains ( $n\text{-C}_6\text{H}_{13}$ ) of three molecules closely gather each other, indicating strong hydrophobic interaction. Besides, there exists electrostatic attraction between the carbazole and the barbituric acid. These two kinds of intermolecular actions work together to limit the rotation of certain bonds in the molecules, and result in the strongest AIE effect of the six compounds.

For compound CB-6, the aggregated form of the N-alkyl chain ( $n\text{-C}_9\text{H}_{19}$ ) is relatively lower relative to CB-5, but there is also a weaker hydrophobic interaction. The backbones of the four molecules in CB-6 distribute in different way and are far from each other, implying no electrostatic attraction between molecules. Therefore, the intermolecular actions of CB-6 are much weaker relative to those of CB-5, due to that  $n\text{-C}_9\text{H}_{19}$  in CB-6 is a larger alkyl chain than  $n\text{-C}_6\text{H}_{13}$  in CB-5, which may hinder the close packing of molecules. In result, the relative loose aggregation of CB-6 explains the lower AIE index relative to CB-5.

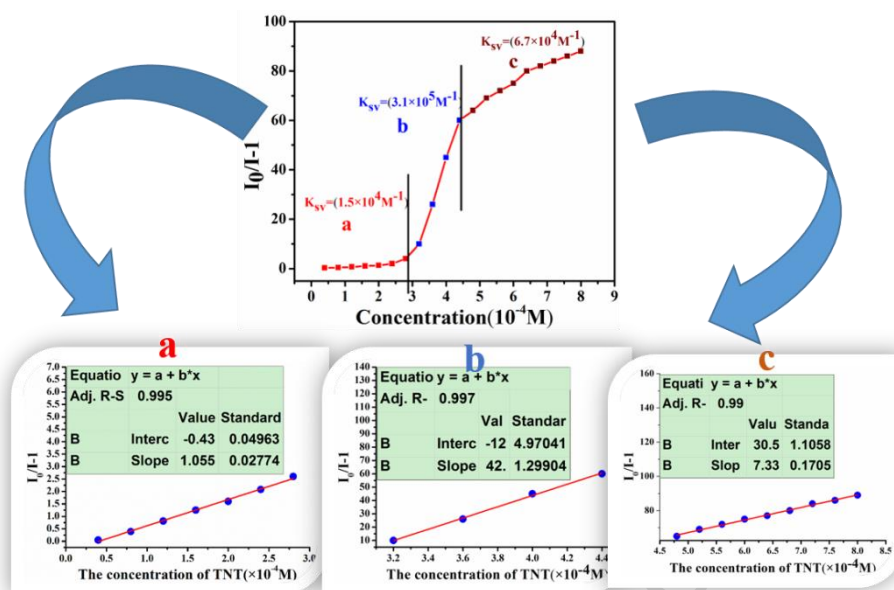
### 3.4 Detection of nitroaromatic explosives



**Fig.5** Fluorescence quenching experiment of TNT in solution of CB-5 ( $f_w = 90\%$ ).

The aggregation of CB-5 in THF/water ( $f_w=90\%$ ) exhibits excellent sensing performance to TNT. As shown in Fig. 5, with the TNT concentration increasing, the fluorescence intensity of CB-5 aggregation gradually decreases. What is noteworthy is that  $\lambda_{em}$  of CB-5 unchanged during TNT addition, meaning that no other compounds was formed.

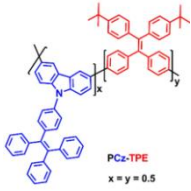
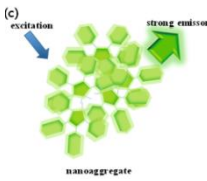
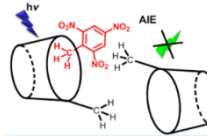
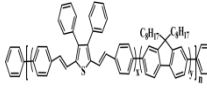
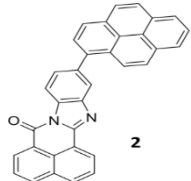
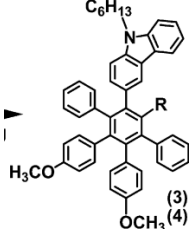
A quenching process can be expressed by Stern-Volmer relationship  $I_0/I = 1 + K_{sv} [Q]$  [21], where,  $I_0$  and  $I$  are the initial and final fluorescence intensity after the addition of TNT respectively,  $[Q]$  is the concentration of TNT, and  $K_{sv}$  is the quenching constants. The plots of  $I_0/I - 1$  versus  $[Q]$  are shown in Fig.6. A good relationship between  $I_0/I - 1$  and  $[Q]$  was obtained with  $[Q]$  increasing from  $3.2$  to  $4.4 \times 10^{-4}$  M, which gives the  $K_{sv}$  value of  $3.1 \times 10^5$  M<sup>-1</sup>. The detection limit is an important parameter for evaluating whether a sensor is sensitive. According to the formula  $LOD = 3S/K_{sv}$ , the limit of detection (LOD) of CB-5 in  $f_w=90\%$  mixture solution for TNT is 0.329 ppb [22, 23].

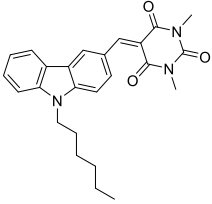


**Fig. 6** Fluorescence quenching Stern-Volmer curve of CB-5 with TNT.

As we know, most of the sensors that detect TNT are based on gas detection. It is still of great importance to detect NACs in wastewater, due to that the residues of TNT and DNT in the environment will cause serious health problems in both animals and humans [24-25]. Because the poor water solubility of most organic sensing material, relatively few fluorescent sensors have been reported for the detection of TNT in water solution. However, some typical AIE sensing materials, which emit strong fluorescence as micro aggregate in aqueous media, have been reported for detecting TNT (Table 3). As found, the  $K_{sv}$  of most of the sensing materials in Table 3 is at the order of  $10^4 K_{sv}/M^{-1}$  [26-31]. Exceptionally, the  $K_{sv}$  of CB-5 is among the highest value with the order of magnitude of  $10^5 K_{sv}/M^{-1}$ . This results indicate the aggregation of CB-5 takes superior performance in detecting TNT in aqueous medium.

**Table 3** Performance comparison of chemosensors reported for TNT

Receptor	Analyte	The type of sensor	Detecting system	$K_{sv}/M^{-1}$	Limit of detection (LOD)	Ref.
	TNT	solution	THF-H <sub>2</sub> O mixtures (1 : 9 v/v)	$8.5 \times 10^4$	7.4 $\mu$ M	[26]
	TNT	solution	THF-H <sub>2</sub> O mixtures (1 : 9 v/v)	$0.8 \times 10^4$		[27]
	TNT	solution	THF-H <sub>2</sub> O mixtures (0.5 : 9.5 v/v)	$1.37 \times 10^5$	0.22 ppb	[28]
	TNT	solution	THF-H <sub>2</sub> O mixtures (0.5 : 9.5 v/v)	$4.45 \times 10^3$	0.14 ppb	[29]
	TNT	solution	THF-H <sub>2</sub> O mixtures (2 : 8 v/v)	$6.0 \times 10^4$	0.25 ppb	[30]
	TNT	solution	THF-H <sub>2</sub> O mixtures (0.5 : 9.5 v/v)	$13 \times 10^5$	0.03 $\mu$ M	[31]

	TNT	solution	THF-H <sub>2</sub> O mixtures (1 : 9 v/v)	$3.1 \times 10^5$	0.33 ppb	This work
---	-----	----------	---	-------------------	----------	--------------

Generally, the mechanisms of fluorescence quenching include Förster resonance energy transfer (FRET) and photoinduced electron transfer (PET). To determine which mechanism plays the main role of quenching process, both the absorption spectrum of TNT and the emission spectrum of CB-5 are compared, as shown in Fig. 7. Observably, there is no overlap between these two spectra, meaning no FRET mechanism to responsible for the quenching. Therefore, the fluorescence quenching of CB-5 are mainly attributed to PET mechanism [32-34].

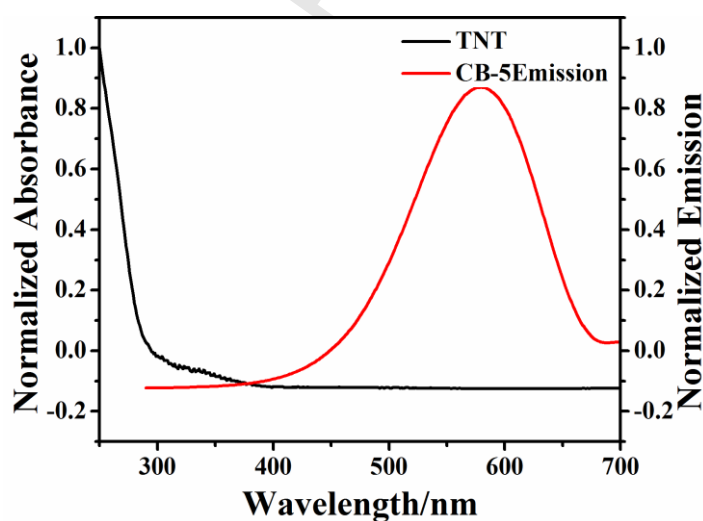


**Fig. 7** Absorption spectrum of TNT and emission spectrum of CB-5.

As shown in Fig. S14, the energy levels and electron cloud distributions of the HOMO and LUMO of TNT and **CB-5** were calculated by the B3LYP/6-325 31G (d)

program. When the excited **CB-5** is exposed to TNT, the excited electrons are transferred from the LUMO of CB-5 to the LUMO of TNT. The main driving force of PET is the difference between the LUMO value of CB-5 and TNT, which is 1.029 V.

Paper-based sensors have attracted great interest because their economics and easy of preparation [35, 36]. Hence, the Paper-based sensor was obtained by soaking a round Whatman filter paper in a solution of CB-5 ( $f_w = 90\%$   $C_{CB-5}=10^{-4}M$ ) with a following drying (Fig. 8A). A round glass bottle containing TNT powder, which provided saturated TNT vapor, was covered with the paper-based sensor. After standing for five minutes, the paper-based sensor were photographed, as shown in Fig. 8B. As observed, a quenched spot corresponding to the bottle appeared, indicating the paper sensor is sensitive to TNT vapor. Another paper sensor was soaked into a solution of TNT in THF ( $C_{TNT}=10^{-4}M$ ), as observed, the whole paper sensor was quenched thoroughly (Fig. 8C). These results showed that this paper sensor base on CB-5 can be used to detect the TNT vapor.

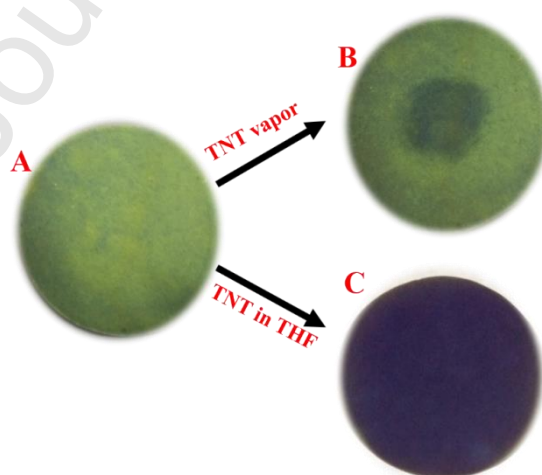


**Fig. 8** A: Paper sensor based on CB-5 ( $f_w = 90\%$ ); B: paper sensor quenched by TNT vapor; C: Paper sensor after soaked in solution of TNT in THF.

#### 4. Conclusion

All the six barbituric acid derivatives with different alkyl substituents show AIE effect. The alkyl substituents play important role in forming aggregates of the compounds. In the compounds with short alkyl substituents (from CB-1 to CB-4), the hydrophobic interaction was negligible, while the electrostatic attraction between the carbazole and the barbituric acid moieties made molecules closely aggregated and resulted in the AIE activity. In the compounds with long alkyl substituents (CB-5 and CB-6), the hydrophobic interaction was remarkable, and steric hindrance of longer alkyl substituents hindered the closely aggregation of the CB-6. CB-5 exhibited the highest AIE index of 49, due to its strong hydrophobic interaction by *n*-hexyl substituent and the good intermolecular electrostatic attraction between the carbazole and the barbituric acid moieties. Based on the enhanced AIE effect, CB-5 showed excellent sensing performance in detecting TNT, which may be used as chemosensor for TNT. Additionally, this work revealed the effect of alkyl length on the properties of AIE, providing a reasonable strategy for the design of AIE molecule.

#### Acknowledgements

This work was financially supported by a Project of Shandong Province Higher Educational Science and Technology Program (NO. J18KZ004), the Natural Science Foundation of Shandong province (ZR2018MB025) and the Funds for Research Leader in Jinan (2018GXRC028).

## References

- [1] Zheng, Z., Li, D., Liu, Z., Peng, H. Q., Sung, H. H., Kwok, R. T., & Tang, B. Z. (2019). Aggregation-Induced Nonlinear Optical Effects of AIEgen Nanocrystals for Ultradeep In Vivo Bioimaging. *Advanced Materials*, 31, 1904799.
- [2] Tu, Y., Yu, Y., Zhou, Z., Xie, S., Yao, B., Guan, S., & Chen, S. (2019). Specific and Quantitative Detection of Albumin in Biological Fluids by Tetrazolate-Functionalized Water-Soluble AIEgens. *ACS applied materials & interfaces*, 11(33), 29619-29629.
- [3] Li, K., Liu, Y., Li, Y., Feng, Q., Hou, H., & Tang, B. Z. (2017). 2, 5-bis (4-alkoxycarbonylphenyl)-1, 4-diaryl-1, 4-dihydropyrrolo [3, 2-b] pyrrole (AAPP) AIEgens: tunable RIR and TICT characteristics and their multifunctional applications. *Chemical science*, 8(10), 7258-7267.
- [4] Pasha, S. S., Yadav, H. R., Choudhury, A. R., & Laskar, I. R. (2017). Synthesis of an aggregation-induced emission (AIE) active salicylaldehyde based Schiff base: study of mechanoluminescence and sensitive Zn (ii) sensing. *Journal of Materials Chemistry C*, 5(37), 9651-9658.
- [5] Wu, H., Pan, Y., Zeng, J., Du, L., Luo, W., Zhang, H., & Qin, A. (2019). Novel Strategy for Constructing High Efficiency OLED Emitters with Excited State Quinone-Conformation Induced Planarization Process. *Advanced Optical Materials*, 1900283.
- [6] Liu, Y. L., Wang, Z. K., Qin, W., Hu, Q. L., & Tang, B. Z. (2017). Fluorescent detection of Cu (II) by chitosan-based AIE bioconjugate. *Chinese Journal of Polymer Science*, 35(3), 365-371.
- [7] Li, S., Wu, M., Kang, Y., Zheng, H. W., Zheng, X. J., Fang, D. C., & Jin, L. P.

- (2019). Grinding-Triggered Single Crystal-to-Single Crystal Transformation of a Zinc (II) Complex: Mechanochromic Luminescence and Aggregation-Induced Emission Properties. *Inorganic chemistry*, 58(7), 4626-4633.
- [8] Ma, C., Zhang, X., Yang, Y., Ma, Z., Yang, L., Wu, Y., & Wei, Y. (2016). Effect of alkyl length dependent crystallinity for the mechanofluorochromic feature of alkyl phenothiazinyl tetraphenylethenyl acrylonitrile derivatives. *Journal of Materials Chemistry C*, 4(21), 4786-4791.
- [9] Kizaki, K., Imoto, H., Kato, T., & Naka, K. (2015). Facile construction of N-alkyl arylaminomaleimide derivatives as intensively emissive aggregation induced emission dyes. *Tetrahedron*, 71(4), 643-647.
- [10] Zheng, M., Sun, M., Li, Y., Wang, J., Bu, L., Xue, S., & Yang, W. (2014). Piezofluorochromic properties of AIE-active 9, 10-bis (N-alkylpheno-thiazin-3-yl-vinyl-2) anthracenes with different length of alkyl chains. *Dyes and Pigments*, 102, 29-34.
- [11] Liu, Y., Lei, Y., Liu, M., Li, F., Xiao, H., Chen, J., & Cheng, Y. (2016). The effect of N-alkyl chain length on the photophysical properties of indene-1, 3-dionemethylene-1, 4-dihydropyridine derivatives. *Journal of Materials Chemistry C*, 4(25), 5970-5980.
- [12] Diao, L., Cui, Y., Li, T., Zhou, L., & Liu, W. (2013). Synthesis and Optical Properties of Some Compounds Based on Carbazole and s-Triazine. *Chemistry letters*, 42(4), 410-412.
- [13] Chen, Y., Wang, Y., Yuan, Y., Jiao, Y., Pu, X., & Lu, Z. (2015). Deactivation mechanism of a novel AIE-active naphthalimide derivative in more polar solutions. *Physical Chemistry Chemical Physics*, 17(2), 1309-1316.

- [14] Hu, Y., Han, T., Yan, N., Liu, J., Liu, X., Wang, W. X., & Tang, B. Z. (2019). Visualization of Biogenic Amines and In Vivo Ratiometric Mapping of Intestinal pH by AIE-Active Polyheterocycles Synthesized by Metal-Free Multicomponent Polymerizations. *Advanced Functional Materials*, 1902240.
- [15] Xu, Z., Gu, J., Qiao, X., Qin, A., Tang, B. Z., & Ma, D. (2019). Highly Efficient Deep Blue Aggregation-Induced Emission Organic Molecule: A Promising Multifunctional Electroluminescence Material for Blue/Green/Orange/Red/White OLEDs with Superior Efficiency and Low Roll-Off. *ACS Photonics*, 6(3), 767-778.
- [16] Berendsen, H. J. C., Postma, J. P. M., Van Gunsteren, W. F., & Hermans, J. (1981). *Intermolecular Forces*, ed. B. Pullman. Dordrecht: Reidel, 331-342.
- [17] Berendsen, H. J. C., Grigera, J. R., & Straatsma, T. P. (1987). The missing term in effective pair potentials. *Journal of Physical Chemistry*, 91(24), 6269-6271.
- [18] Wiedemair, M. J., & Hofer, T. S. (2017). Towards a dissociative SPC-like water model—probing the impact of intramolecular Coulombic contributions. *Physical Chemistry Chemical Physics*, 19(47), 31910-31920.
- [19] Sun, H., Ren, P., & Fried, J. R. (1998). The COMPASS force field: parameterization and validation for phosphazenes. *Computational and Theoretical Polymer Science*, 8(1-2), 229-246.
- [20] Sun, H. (1998). COMPASS: an ab initio force-field optimized for condensed-phase applications overview with details on alkane and benzene compounds. *The Journal of Physical Chemistry B*, 102(38), 7338-7364.
- [21] Ma, X., Tao, F., Zhang, Y., Li, T., Raymo, F. M., & Cui, Y. (2017). Detection of nitroaromatic explosives by a 3D hyperbranched  $\sigma$ - $\pi$  conjugated polymer based on

- a POSS scaffold. *Journal of Materials Chemistry A*, 5 (27), 14343-14354.
- [22] Shyamal, M., Maity, S., Mazumdar, P., Sahoo, G. P., Maity, R., & Misra, A. (2017). Synthesis of an efficient Pyrene based AIE active functional material for selective sensing of 2, 4, 6-trinitrophenol. *Journal of Photochemistry and Photobiology A: Chemistry*, 342, 1-14.
- [23] Chemate, S., Erande, Y., Mohbiya, D., & Sekar, N. (2016). Acridine derivative as a “turn on” probe for selective detection of picric acid via PET deterrence. *RSC Advances*, 6(87), 84319-84325.
- [24] Wang, D. H., Cui, Y. Z., Tao, F. R., Niu, Q. F., Li, T. D., & Xu, H. (2016). A novel film of conjugated polymer grafted onto gelatin for detecting nitroaromatics vapor with excellent inhibiting photobleaching. *Sensors and Actuators B: Chemical*, 225, 319-326.
- [25] Wang, A. Q., Cui, Y. Z., Tao, F. R., Wang, D. H., Li, T. D., & Xu, J. K. (2016). Preparation of a functionalized glass sensor and its sensing performances for nitroaromatics. *Thin Solid Films*, 598, 299-304.
- [26] Dong, W., Ma, Z., Chen, P., & Duan, Q. (2019). Carbazole and tetraphenylethylene based AIE-active conjugated polymer for highly sensitive TNT detection. *Materials Letters*, 236, 480-482.
- [27] Shin, B., Sohn, H., & Yoo, H. W. (2018). Optical Characterization of Germole Nanoaggregates and Its Explosive Sensing Application. *Journal of the Korean Physical Society*, 73(7), 908-911.
- [28] Liu, Y., Zhang, Q., Jing, D., He, X., Cui, S., & Liu, Y. (2019). Rapid visual

- identification of nitroaromatics compounds by aggregation-induced enhanced emission fluorescent assays with a Cd (II)-H3BTT complex. *Sensors and Actuators B: Chemical*, 126623.
- [29] Adil, L. R., Gopikrishna, P., & Krishnan Iyer, P. (2018). Receptor-free detection of picric acid: a new structural approach for designing aggregation-induced emission probes. *ACS applied materials & interfaces*, 10(32), 27260-27268.
- [30] Dong, W., Ma, Z., Chen, P., & Duan, Q. (2019). Carbazole and tetraphenylethylene based AIE-active conjugated polymer for highly sensitive TNT detection. *Materials Letters*, 236, 480-482.
- [31] Boonsri, M., Vongnam, K., Namuangruk, S., Sukwattanasinitt, M., & Rashatasakhon, P. (2017). Pyrenyl benzimidazole-isoquinolinones: Aggregation-induced emission enhancement property and application as TNT fluorescent sensor. *Sensors and Actuators B: Chemical*, 248, 665-672.
- [32] Georgiev, N. I., Bakov, V. V., & Bojinov, V. B. (2019). A Solid-State-Emissive 1, 8-Naphthalimide Probe Based on Photoinduced Electron Transfer and Aggregation-Induced Emission. *ChemistrySelect*, 4(14), 4163-4167.
- [33] Kaur, M., Mehta, S. K., & Kansal, S. K. (2017). A fluorescent probe based on nitrogen doped graphene quantum dots for turn off sensing of explosive and detrimental water pollutant, TNP in aqueous medium. *Spectrochimica Acta Part A: Molecular and Biomolecular Spectroscopy*, 180, 37-43.
- [34] López-Marzo, A. M., & Merkoçi, A. (2016). Based sensors and assays: a success of the engineering design and the convergence of knowledge areas. *Lab on a Chip*, 16(17), 3150-3176.

- [35] Ahmed, S., Bui, M. P. N., & Abbas, A. (2016). Based chemical and biological sensors: Engineering aspects. *Biosensors and Bioelectronics*, 77, 249-263.
- [36] Cunningham, J. C., DeGregory, P. R., & Crooks, R. M. (2016). New functionalities for paper-based sensors lead to simplified user operation, lower limits of detection, and new applications. *Annual Review of Analytical Chemistry*, 9, 183-202.

Journal Pre-proof

### **Declaration of Interest Statement**

The authors declare that there is no conflict of interest regarding the publication of this paper.

Journal Pre-proof

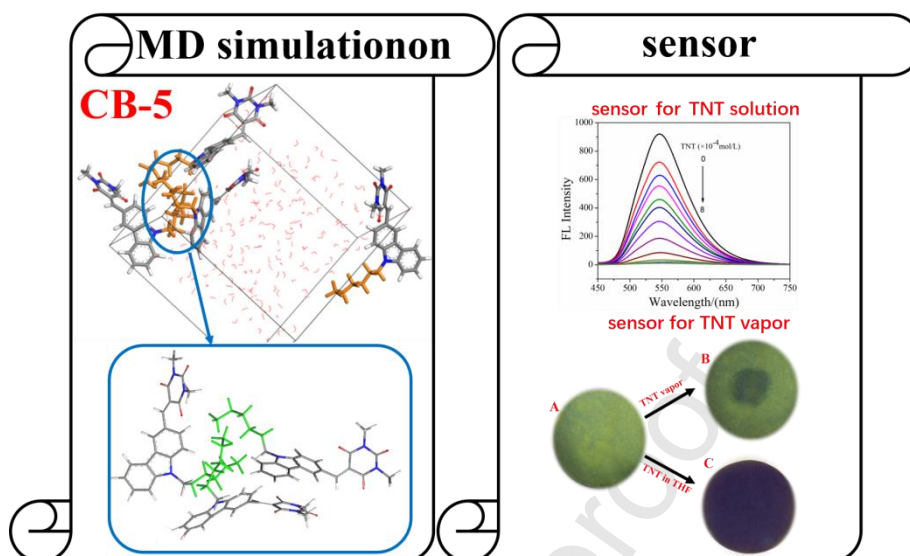
### **Author Biography**

**First author: Hanjun Zhang** working toward a M.S. degree in School of Chemistry Qilu University of Technology.

**Yue-Zhi Cui** received her PhD degree in 2004 at Shandong University, China. She is currently a professor at Qilu University of Technology. Her research interests are in the areas of materials chemistry and chemosensor.

**Zhen Xu** received her PhD degree in 2004 at Shandong University, China. She is currently a professor at Qilu University of Technology.

## Graphical Abstract



Molecular dynamics simulation exhibited that the hydrophobic interaction of the alkyl chain formed aggregates and produced a strong AIE effect. The aggregate CB-5 showed a superior performance in detecting TNT in aqueous media and vapor.

**Highlights:**

- Six novel AIE barbituric acid derivatives were designed.
- Visualization of AIE process was illustrated by molecular dynamics simulation.
- The hydrophobic interaction of the alkyl chain formed aggregates.
- The CB-5 exhibited a superior performance in detecting TNT in aqueous media.
- The paper sensor based on CB-5 showed a superior sensitivity toward TNT.

Journal Pre-proof